Vehicle X-Ray Images Registration

Abraham Marciano[1, 2] *, Laurent D. Cohen[1], Najib Gadi[2]

[1] Université Paris-Dauphine, PSL Research University, CNRS, UMR 7534, CEREMADE, 75016 Paris, France
[2] Smiths Detection, 94405 Vitry-sur-Seine, France
marciano@ceremade.dauphine.fr

Abstract. Image registration is definitely one of the most prominent techniques at the heart of computer vision research. Applications range from medical image analysis, remote sensing or robotics to security-related tasks such as surveillance or motion tracking. In our previous work, a solution was provided to address the registration problem involving top-view radiographic images of vehicles. A unidimensional minimization scheme was formulated along with a column-wise constancy constraint on the displacement field.
In this paper, we show that the proposed method is not sufficient in case of significant vertical shifts between the cars of both moving and static images. In fact, the radiated beam is triangular, thus any translated object is projected differently according to its distance to the x-ray source. We therefore add a 1D unconstrained optimization to the previous scheme for a y-direction correction. We also demonstrate that applying the vertical correction following our 1D optimization in the x-axis yields better results than performing a simultaneous minimization on both components.
Finally, the possible apparition of artefacts in the deformed image throughout the optimization process is analyzed. Diffusion and volume-preserving schemes are considered and compared in this regard.

Keywords: Image Registration, Variational Approach, Energy Minimization Methods, Difference Detection, Volume Preservation.

1 Introduction

Security is imposing itself as one of the most defining stakes in modern societies. Massive investments have been dedicated to find innovative solutions in order to assist the military or custom officers in their tasks. Image processing and computer vision methods are utterly ubiquitous in defense industries and provide wide-ranging applications.

Image registration is commonly referred to as the searching process of a transformation that aligns, in an optimal but "plausible" way, a moving image $\boldsymbol{T}$ with a static image $\boldsymbol{R}$ [1, 2].

Aiming at automatic threat targeting, the registration problem of top-view x-ray scans of same-model vehicles was introduced in our previous work [3]. A straightforward solution was proposed to address the nonlinear deformations issue: a unidimensional optimization scheme with a constancy constraint formulated for each column of the displacement field.

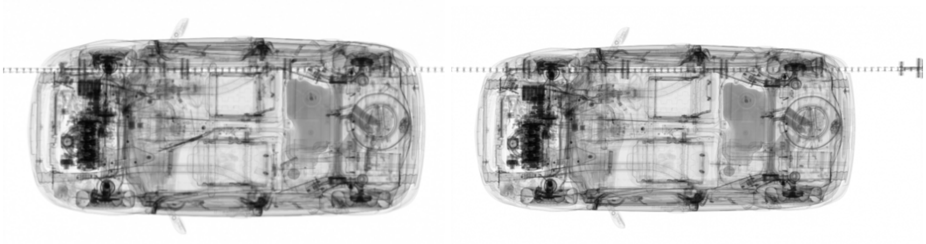

(a)

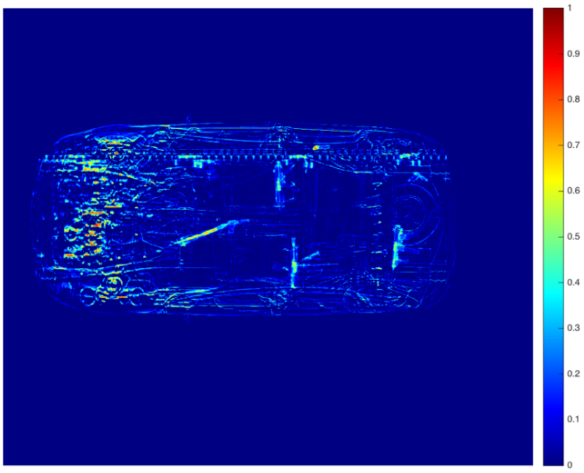

(b)

Fig. 1. (a) ***R*** containing threats and ***T***; (b) the normalized difference map following pose estimation and unidimensional registration on x-axis. The substantial vertical shift between both acquisitions entails alignment artefacts, particularly on the front part where inspection is impossible.

Yet, this assumption doesn't hold in case of significant translation between both scanned cars in the vertical axis. The beam emitted from the source located at the center of the detection line is indeed triangular (see **Fig. 2.**). Hence, any shift may be impacted differently in the projection image, according to the distance separating the source from the object.
In **Fig. 1.** for instance, registration artefacts at the front region prevent any threat detection capacity.

Horizontal and vertical deformations being of a different nature, instead of employing "blind" non-rigid registration models, we provide a method based on the separate analysis of horizontal and vertical deformation phenomena (inherent to the scanning system features).

In this paper, we will briefly give an outline of the main energy-minimization based registration methods along with their numerical solutions.

A second part will describe the registration issue while scanning shifted cars. Then, we will show that performing a post-processing elastic registration over the vertical component of the displacement field yields satisfactory results. We will also demonstrate that the approach combining successive optimizations on horizontal and vertical components is preferable to a simultaneous minimization approach.

2 Outline of Non-Linear Registration Methods

2.1 Mathematical Problem Setup

Let's consider a static image $\boldsymbol{R}$ and a moving template $\boldsymbol{T}$; we look for a transformation applied on $\boldsymbol{T}$ such that both images align as closely as possible [1, 2]. The general formulation is given by the definition of $\boldsymbol{R}$ and $\boldsymbol{T}$ as d-dimensional images represented by the mappings $\boldsymbol{R}, \boldsymbol{T}: \Omega \longrightarrow \mathbb{R}, \Omega \in [0,1]^d$ in normalized coordinates. The transformation ϕ is expressed via the displacement field $\boldsymbol{u}$: $\Omega \longrightarrow \mathbb{R}^d$ with $\phi = id + \boldsymbol{u}$.

Hence, given $\boldsymbol{x} \in \Omega$, the transformed image is written $\boldsymbol{T}\big(\phi(\boldsymbol{x})\big) = \boldsymbol{T}\big(\boldsymbol{x} + \boldsymbol{u}(\boldsymbol{x})\big)$ where $\boldsymbol{u}$ is applied on the position $\boldsymbol{x}$ of $\boldsymbol{T}$. In other words, $\boldsymbol{T}(\boldsymbol{x})$ is the intensity of $\boldsymbol{T}$ at $\boldsymbol{x}$ and $\boldsymbol{T}\big(\boldsymbol{x} + \boldsymbol{u}(\boldsymbol{x})\big)$ designates the value of $\boldsymbol{T}$ at the translated position.

Since we wish to minimize the distance between $\boldsymbol{T} \circ \phi$ and $\boldsymbol{R}$, the unified optimization framework for intensity-based registration is given by the following joint functional scheme:

Find u minimizing

$$\mathcal{J}[u] = \mathcal{D}[\boldsymbol{T}(\boldsymbol{u}), \boldsymbol{R}] + \alpha \mathcal{S}[\boldsymbol{u}] \tag{1}$$

where $\mathcal{D}$ is referred to as the distance measure between $\boldsymbol{T} \circ \phi$, the transformed image, and $\boldsymbol{R}$. It commonly designates the data-fitting term or external force [4] to obtain an ideal alignment.

In order to tackle the ill-posedness of the optimization problem ([1, 2]), a regularization term $\mathcal{S}$ is introduced (internal force [4]). It is designed to keep the displacement smooth during deformation by penalizing unwanted or implausible solutions. The regularization strength is controlled by the smoothing parameter α: increasing its value emphasizes the smoothness of $\boldsymbol{u}$ and vice-versa. The choice of this parameter has been studied but remains utterly dependent on the considered application and the appreciation of the operator ([5-7]).

Similarly, both data-fitting and smoothing terms are selected according to the specificity of the registration task. The most popular similarity measure is the *Sum of Squared Differences* (*SSD*). The *Normalized Cross Correlation* (*NCC*) is also widespread for matching problems of images sampled with the same modality. Information-theoretic approaches based on Shannon's entropy are employed for multimodal registration (*Mutual Information – MI*). Over the years, more sophisticated measures have also been explored such as the so-called *NGF- Normalized Gradient Fields.* See [1], [2], or [7] for further details about similarity measures.

In various registration tasks, the choice of the smoothing term is crucial ([1]). It allows the embedding of physical priors or possible acquisition constraints within the optimization scheme. The next section will depict a larger overview of the most widespread regularization terms.

Note that the selection of both terms is conditioned upon the existence of a Gâteaux derivative ([1, 2, 7, 8])

2.2 Registration Methods

Registration can be landmark-base, i.e. the image is transformed via the matching of sparse elements (feature points or manually annotated control landmarks) combined with TPS (Thin-Plate-Spline) interpolation to yield dense correspondences ([1, 2, 6]). Although these methods have proven their efficiency in many applications e.g. in medical image analysis, they show less flexibility than the unified variational framework introduced in (1) (see [4]). In addition, despite the recent achievements on key points automatic generation (deep-learning based), unmanned landmark detection remains a challenging task.

For these reasons, we chose to focus our work on intensity-based or so-called iconic methods. These approaches generally split into two categories ([1, 2, 6]).

Regarding parametric image-registration techniques (*PIR*), the displacement field $\boldsymbol{u}$ is parametrized. The optimization process thereby consists in finding the parameters minimizing $\mathcal{J}$. In B-spline approaches, the displacement is defined as a linear combination of a small set of basis functions. See ([2, 6]) for a further description of *PIR* approaches. In general, the smoothing terms are chosen such that $\mathcal{S}[u] = 0$ with a parametrization meant to implicitly integrate regularization constraints. Though, Tychonov regularization may often be used.

In non-parametric approaches (*NPIR*), the smoothing term plays a major role while the displacement is no longer parametrized. Most common techniques employ *L2*-normed terms: diffusion, elastic, curvature or fluid regularizers ([2, 4]). The demons method [9] is inspired from optical-flow techniques, where a Gaussian smoothing applied at each iteration falls within a diffusion-like regularization ([4]). Topology-preserving registration is also a very active field of research. In fluid mechanics, incompressibility imposes that the determinant of the transformation Jacobian remains equal to one (see e.g. [6]). On this basis, Rohling [10] and Christensen [11] add a soft constraint to (1): $\|\det(Id + \nabla\boldsymbol{u}) - 1\|^2$ or its logarithmic version to ensure volume preservation (various regularizers are also described in [10-12]). Instead, Haber and Modersitzki opt for an inequality/equality hard constraint (resp. [8] and [7]). More recently, Rueckert et al. compare soft and hard-constraint techniques in [13].

Alternative approaches concentrate on the diffeomorphic framework. ϕ is then explicitly constrained to be a continuously differentiable bijection having a smooth inverse. The deformation is modeled via a time-dependent velocity vector field. See [13], the LDMM model [14] or the earlier work of [15] for detailed explanations about these schemes. See also the recent contributions of Mang et al. about mass and volume preservation constraints for a comprehensive state of the art overview ([16, 17]).

Other methods suggest to apply a post-processing step over the displacement field after registration. In [18], Poisson's equation is solved to maintain a so-called solenoidal displacement field $\boldsymbol{u}$ and maintain the preservation of volumes.

Similarly, rigidity constraints (hard and soft versions) have been formulated in different publications. Though, they are beyond the scope of this paper (see [19] for instance).

2.3 Numerical Solutions

In [1, 2], Modersitzki suggests a general optimization framework to solve (1). An approximation of the Gauss-Newton method is employed, usually combined with a multilevel strategy as well as a backtracking line-search method to yield an optimal step size at each iteration [2]. Matrix-free approaches are also proposed to speed-up the computations ([2, 20]). The variations of the displacement between consecutive iterations are estimated by $\|\nabla \boldsymbol{u}\|_2$in order to stop the minimization process whenever it falls under a pre-set threshold ϵ. See [1, 2] for further details about the stopping criterion.

Alternative numerical techniques have also been presented for computationally-demanding problems. See [2] on *l*-BFGS or Trust-Region methods that can achieve fast quadratic convergence.

For volume-preserving constrained problems, Modersitzki et al. resort to the framework of Sequential Quadratic Methods (SQP) [7] or a variant of the log-barrier method [8].

Diffeomorphic image registration as described in [13, 14] typically uses an implicit regularization (by solving a Poisson *pde*) while gradient-descent methods are used to find an optimal solution. In their latest works, Mang et al. [15] proposed second-order numerical methods to produce diffeomorphic mappings.

In [1, 2], a discretize-then-optimize approach is used. In several applications, the choice of discretization paradigms is crucial. Staggered, nodal or cell-centered grids may be used. See [2] for more details about interpolation or discretization issues.

For an in-depth description and analysis of registration methods, please refer to [6].

3 Problem Presentation

3.1 1D Horizontal Correction Scheme Remainder

In our previous work [3], we demonstrated that rigid registration was not sufficient for top-view scans of vehicles obtained by the Smiths Detection HCVL system. Actually, despite the intrinsic rigidity of cars, non-linear deformations may occur as a result of shocks between the conveyor rollers and the back wheels. The issue was simply addressed by applying a rigid pre-processing registration (similarity pose estimation) and then running a 1D registration scheme assuming:

i. a column-wise constancy condition on the displacement field
ii. a negligible vertical component

By combining i. and ii. we had:

$$\boldsymbol{u} = (u_x(x), 0) \tag{2}$$

Eventually, using an *SSD* distance and a diffusion regularization, we formulated (1) as follows:

$$\text{Find } u_x(x) \text{ minimizing}$$

$$\mathcal{J}[u_x] = \frac{1}{2}\left\|\boldsymbol{T}(u_x) - \boldsymbol{R}\right\|_2^2 + \frac{1}{2}\alpha\left\|\nabla_x u_x\right\|_2^2 \tag{3}$$

These assumptions hold in most cases and yield nice registration results. See [3] for a numerical and visual appraisal of the method. Yet, in some situations, the registration accuracy achieves lower performances, as depicted in the next section.

3.2 Necessity for a Vertical Correction

In fact, the scanning system allows for an additional degree of freedom: the car translation along the trailer width (**Fig. 3.**). Besides, the x-ray source is located at the detection line center and generates a pyramidal beam. Any significant translation w.r.t the other image therefore leads to important deformations in the y-axis. More particularly, the deformation magnitude depends on the distance/depth separating the radioactive source from the scanned object as shown in **Fig.2.** Hence, hypothesis ii. is not anymore valid in this situation.

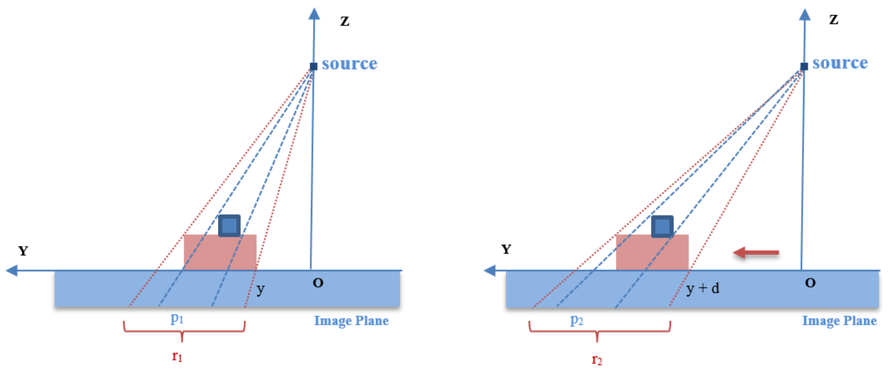

Fig. 2. Vertical shift effect description. The projected distances r_2 and p_2 after displacement are larger than r_1 and p_1. Similarly to the stereovision problem, this difference grows with the object proximity to the x-ray source: $p_2 / p_1 > r_2 / r_1$

These deformations may require either small or even larger scale corrections as shown in **Fig. 1**.

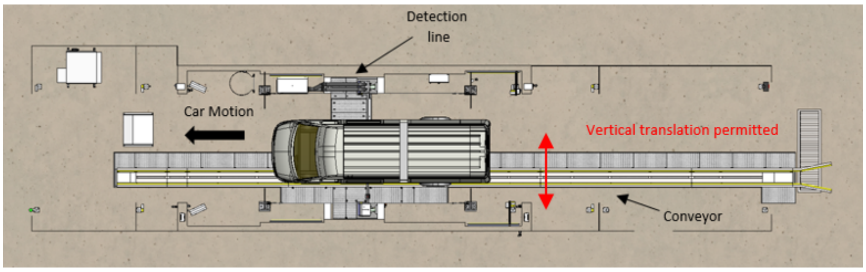

Fig. 3. Top-view of the HCVL system. Translations are permitted along the conveyor width

4 Vertical Correction Solution

4.1 Solution Description

Remaining in the variational framework, we simply intend to apply a supplementary 1D registration over the vertical component of the displacement field. Unlike our previous scheme exposed in sect. **3.1**, we do not assume any specific priors or constraints on the vertical displacement component since the required correction varies accordingly to the objects depth (**Fig. 2.**). A row-wise constancy restriction on u_y is therefore irrelevant. Hence,

$$\boldsymbol{u} = (0, u_y(x, y)) \tag{4}$$

With a diffusion regularizer, (1) is written as follows:

$$\text{Find } u_y(x, y) \text{ minimizing}$$

$$\mathcal{J}[u_y] = \frac{1}{2}\left\|\boldsymbol{T}(u_y) - \boldsymbol{R}\right\|_2^2 + \frac{1}{2}\alpha\left\|\nabla u_y\right\|_2^2 \tag{5}$$

A volume-preserving approach is also tested by adding a soft constraint to the above formula. The joint functional is then given by:

$$\text{Find } u_y(x, y) \text{ minimizing}$$

$$\mathcal{J}[u_y] = \frac{1}{2}\left\|\boldsymbol{T}(u_y) - \boldsymbol{R}\right\|_2^2 + \frac{1}{2}\alpha\left\|\nabla u_y\right\|_2^2 + \frac{1}{2}\beta\left\|\det(\nabla u_y + Id) - 1\right\|_2^2 \tag{6}$$

The soft constrained approach ([10, 11]) is preferred over hard constraints or diffeomorphisms because of its flexibility and implementation simplicity. The β parameter allows control over the balance between diffusion registration and more stringent volume preservation constraints. In alternative methods, parameter tuning turns into a tougher task.

We also wish to compare both simultaneous and successive optimization paradigms for horizontal and vertical corrections. Let's therefore formulate the above problems in two dimensions, maintaining the column-wise constancy constraint for the horizontal component of the displacement field. Thus, let's consider for $(x, y) \in \Omega$:

$$\boldsymbol{u} = (u_x(x), u_y(x,y)) \tag{7}$$

The 2D version of the diffusion registration (7) is given by:

Find $\boldsymbol{u}$ minimizing

$$\mathcal{J}[\boldsymbol{u}] = \frac{1}{2}\|\boldsymbol{T}(\boldsymbol{u}) - \boldsymbol{R}\|_2^2 + \frac{1}{2}\alpha(\|\nabla u_x\|_2^2 + \|\nabla u_y\|_2^2) \tag{8}$$

The two-dimensional volume-preserving optimization scheme is also written as follows:

Find $\boldsymbol{u}$ minimizing (9)

$$\mathcal{J}[\boldsymbol{u}] = \frac{1}{2}\|\boldsymbol{T}(\boldsymbol{u}) - \boldsymbol{R}\|_2^2 + \frac{1}{2}\alpha\left(\|\nabla u_x\|_2^2 + \|\nabla u_y\|_2^2\right) + \frac{1}{2}\beta\|\det(\nabla\boldsymbol{u} + Id) - 1\|_2^2$$

4.2 Numerical Resolution

We will describe the numerical resolution of the 2D problems (8) and (9). The resolution of (5) and (6) is then straightforward since it amounts to exclusively optimizing the vertical displacement field component after obtaining an optimal u_x^* by solving (3).

In the meantime, we resort to first-order minimization methods. Yet, in a future work, we may consider Gauss-Newton methods for speed purposes.

For the diffusion-regularization problem (10), the directional derivatives of the joint functional are given by:

$$\nabla_u\mathcal{J}[\boldsymbol{u}] = \boldsymbol{\nabla T}\big(\boldsymbol{x} + \boldsymbol{u}(\boldsymbol{x})\big)\Big(\boldsymbol{T}\big(\boldsymbol{x} + \boldsymbol{u}(\boldsymbol{x})\big) - \boldsymbol{R}(\boldsymbol{x})\Big) - \alpha\Delta\boldsymbol{u} \tag{10}$$

with $\boldsymbol{x} = (x, y) \in \Omega$ and $\boldsymbol{u}$ as defined in (7). See [1] for a comprehensive demonstration of the Gâteaux derivatives result.

Let's now look at the volume-preserving soft constraint introduced in (9). With a linearization approximation, valid for small displacements, we get:

$$\det(\nabla\boldsymbol{u} + Id) - 1 \approx \partial_x u_x + \partial_y u_y = \operatorname{div}(\boldsymbol{u}) \tag{11}$$

Consequently, the directional derivatives computation yields the following result:

$$\nabla_u\mathcal{J}[\boldsymbol{u}] = \boldsymbol{\nabla T}\big(\boldsymbol{x} + \boldsymbol{u}(\boldsymbol{x})\big)\Big(\boldsymbol{T}\big(\boldsymbol{x} + \boldsymbol{u}(\boldsymbol{x})\big) - \boldsymbol{R}(\boldsymbol{x})\Big) - \alpha\Delta\boldsymbol{u} - \beta\boldsymbol{\nabla}.\operatorname{div}(\boldsymbol{u}) \tag{12}$$

which actually corresponds to the derivative of the elastic registration functional (see [4]). In fact, by noting $\beta = \alpha + \gamma$ we retrieve the well-known Lamé coefficients α and γ. See the appendix in Albrecht et al.'s paper [21] for a detailed demonstration on how to obtain (12).

As in our previous work [3], a gradient-descent method is combined with a multiscale approach to avoid convergence at local minima. We usually run the descent algorithm with a 4-levels Gaussian pyramid. Armijo's backtracking line-search technique is also integrated into the process to yield an optimal step size for each update of $\boldsymbol{u}$.

Both α and β are defined for each scale by fixing desired ratios r_α and r_β between the data fitting term and the regularizers (small ratios indicate large regularization and vice versa). The parameters are estimated at the first iteration and hold for the whole level.

The optimization process is stopped as soon as the displacement variation $\|\nabla \boldsymbol{u}\|_2$ falls below $\epsilon = 10^{-4}$. Computations are performed on a 8 Go RAM - 3,1 GHz Intel Core i7 MacBook. The average calculation time on 992×1186 images with MATLAB 2016b is about 50 s for the successive minimization scheme and reaches more than two minutes for the simultaneous one (no MEX files used so far).

In the next section, we present the results of both approaches for a simultaneous and consecutive optimization fashion.

5 Results

In this chapter, we will use the example brought in **Fig. 1.** and focus on the front part of the vehicle for a visual and numerical assessment of the different techniques.

5.1 Horizontal-then-Vertical Optimization

In **Fig. 4.** and **Fig. 5**, we observe that the smoothing parameters/ratios must be chosen carefully. A too large regularization entails a poor registration accuracy (**Fig. 4.** and **Fig. 5.** (a)**)** while a too soft smoothing makes objects disappear in the difference map. In this case, the threat cannot be longer detected (**Fig. 4.** (c), more explanations are given in subsect. **5.3**). Overall, elastic registration yields better results in terms of threat visualization and MSE measures, as detailed in **Table 1.**.

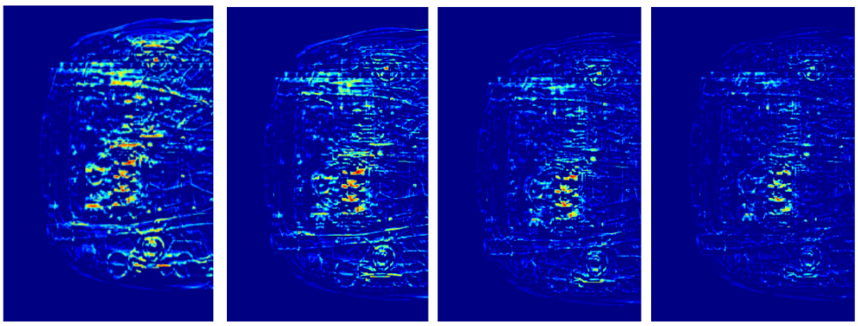

(a) (b) (c) (d)

Fig. 4. (a) Front part difference map after 1D horizontal correction; Diffusion Registration with various parameters - $r_\beta = \infty$ (b) $r_\alpha = 0.1$; (c) $r_\alpha = 1$; (d) $r_\alpha = 2.5$

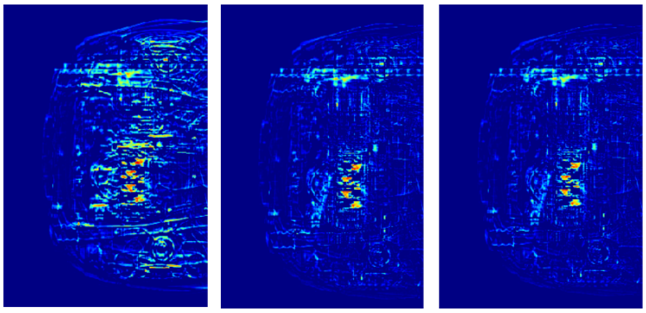

(a) (b) (c)

Fig. 5. Elastic Registration – maps of differences with various parameters (r_α, r_β) (a) $(1, 0.1)$; (b) $(1.5, 2)$; (c) $(2.5, 1)$

In **Fig. 5.** (c), the addition of a vertical "volume-preserving" constraint gives an accurate and reasonable difference map in contrast with the output obtained with the same r_α ratio in **Fig. 4.** (d).

Table 1. Mean Square Error measures obtained with the different regularization ratios

	r_α	r_β	MSE
diffusion	0.1	∞	3.68E-03
	1	∞	1.53E-03
	2.5	∞	7.81E-04
elastic	1	0.1	4.21E-03
	2.5	1	1.38E-03
	1.5	2	1.54E-03

5.2 Simultaneous Optimization

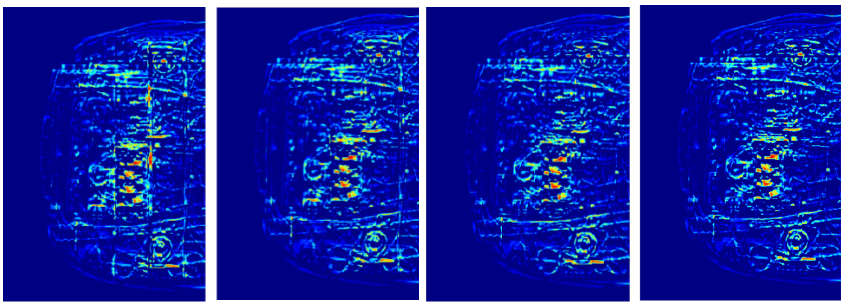

(a) (b) (c) (d)

Fig. 6. Post-registration difference maps with different parameters – (r_α, r_β) (a) $(1, \infty)$; (b) $(1.5, 2)$; (c) $(2.5, 1)$; (d) $(3, 3)$

As depicted in **Fig. 6.**, we get “cleaner” difference maps with the horizontal-then-vertical registration approach where the columns are first rectified to enable a further vertical correction. In addition, by using analogous parameters, the simultaneous method yields larger MSE distances after convergence.

Table 2. Mean Square Error measures obtained with the different regularization ratios

	r_α	r_β	**MSE**
diffusion	1	∞	4.59E-03
elastic	1.5	2	4.41E-03
	2.5	1	4.41E-03
	3	3	3.80E-03

5.3 Further Observations

As mentioned, regularization should be tuned carefully, a too weak smoothing may give a better registration accuracy at the expense of unreasonable deformations. This is especially true when the algorithm tends to deform $\boldsymbol{T}$ in a non-diffeomorphic fashion to “imitate” the added objects in $\boldsymbol{R}$.

Fig. 7. describes the resulting difference map with a weakly-regularized registration. The transformation is piecewise-constant (**Fig. 7.** (b)), meaning that, in a given column, a pixel in the original image $\boldsymbol{T}$ is repeated several times in the deformed $\boldsymbol{T_{final}}$. It actually corresponds to a non-bijective, or more generally: a non-diffeomorphic transformation.

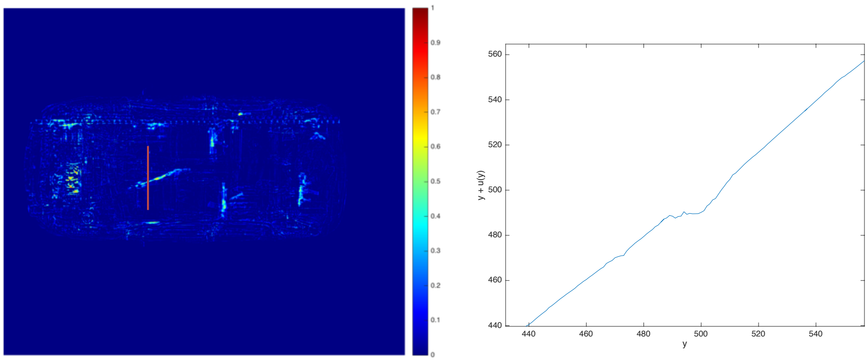

(a) (b)

Fig. 7. Elastic Registration with low smoothing $r_\alpha = 5$, $r_\beta = 5$ (a) difference map; (b) $y + u_y(x, y)$ transformation representation on localized 1D-cross-section

By using proper parameters, we prevent the transformation from being non-diffeomorphic. See the localized 1D-cross section of ϕ in **Fig. 8.** (b): the curve is smoother and strictly increasing.

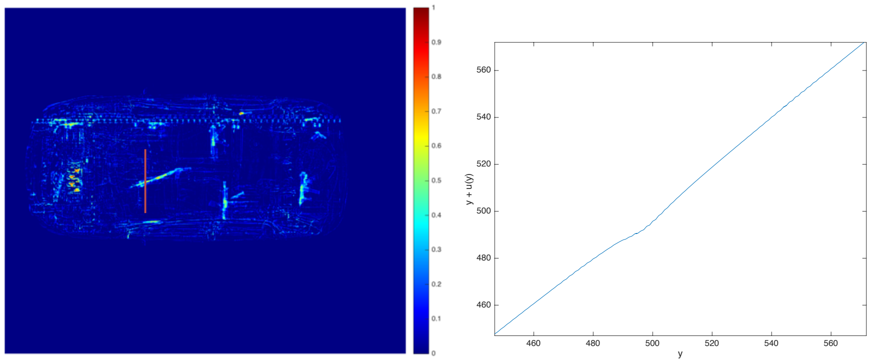

(a) (b)

Fig. 8. Elastic Registration with stronger smoothing r_α = 1.5, r_β = 2 (a) difference map; (b) $y + u_y(x, y)$ transformation representation on localized 1D-cross-section

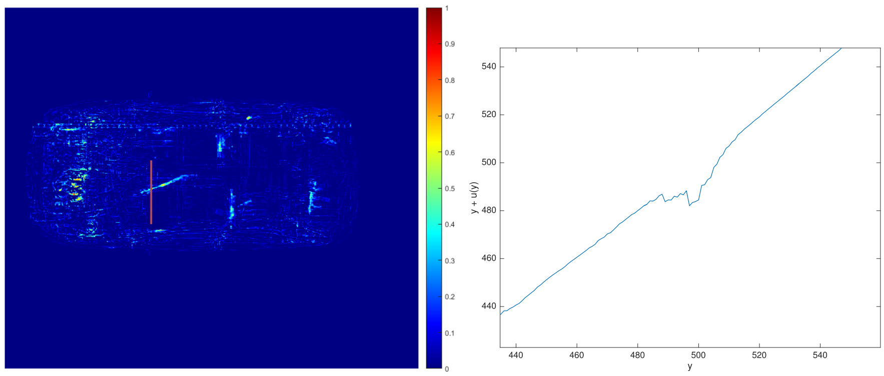

(a) (b)

Fig. 9. Diffusion Registration with r_α = 1.5, r_β = ∞ (a) difference map; (b) $y + u_y(x, y)$ transformation representation on localized 1D-cross-section

In **Fig. 9**., we show the relevance of the additional volume-preserving soft constraint with respect to the diffusion registration result. On a visual aspect, the preservation of volumes is not maintained, leading to a weaker detectability of objects in the difference map. The transformation ϕ lacks regularity and is clearly non-diffeomorphic.

An additional example depicting the registration of images of a carrier is given in **Fig. 10.**

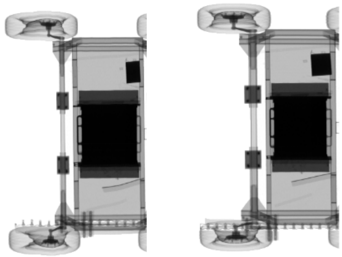

(a)

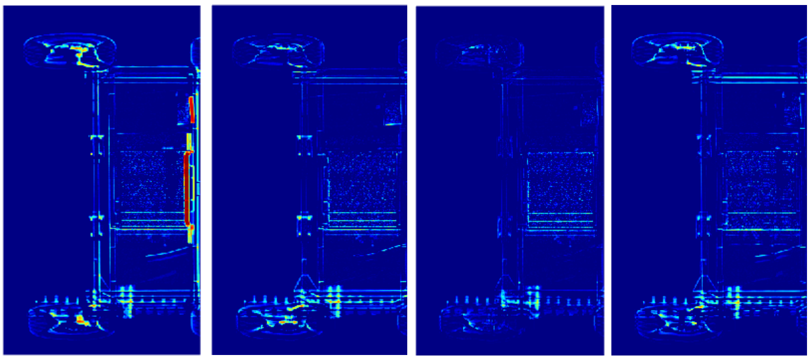

(b) (c) (d) (e)

Fig. 10. (a) ***R*** and ***T***; Difference maps following: (b) rigid registration, (c) 1D horizontal correction, (d) horizontal-then-vertical registration, (e) simultaneous registration with $r_\alpha = 1.5$, $r_\beta = 2$

On this simpler image set too, the consecutive minimization scheme generally shows a better correction than the simultaneous approach. Visually, the major differences at the wheels or the frame borders are removed. It also achieves the lowest MSE (**Table. 3.**).

Table. 3. Mean Square Error measures obtained with the different registration methods

	Rigid Registration	**X-axis Correction**	**X-then-Y Correction**	**Simultaneous**
MSE	1.55E-02	4.14E-03	1.11E-03	4.90E-03

After validating our method on hundreds of scan pairs, we empirically obtain stable and accurate results with the ratio parameters $r_\alpha = 1.5$, $r_\beta = 2$ for an optimal detectability of the objects of interest targeted. In **Fig. 11.** and **Table. 4.**, an additional illustration of our method performances is given.

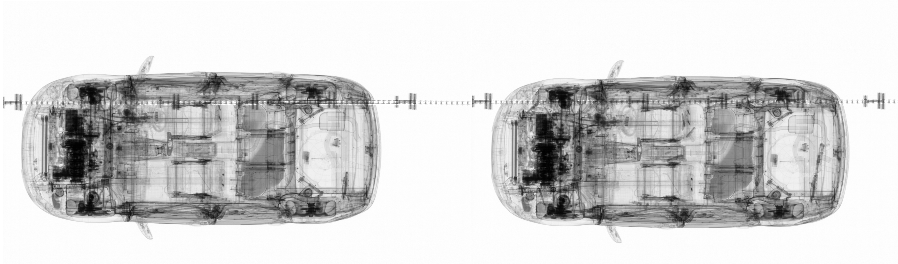

(a)

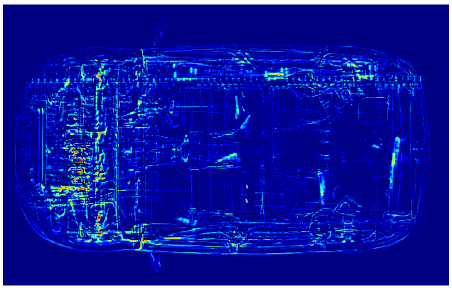

(b)

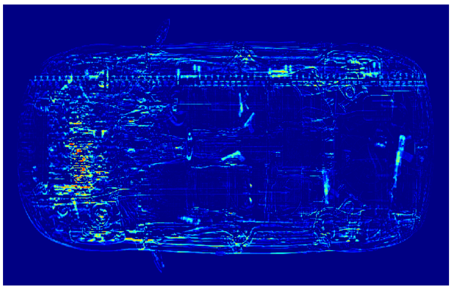

(c)

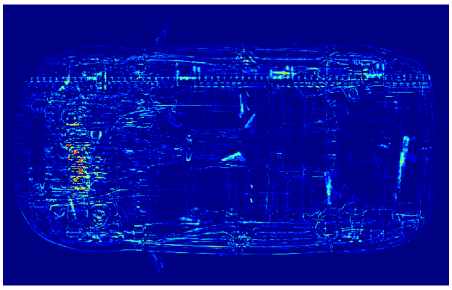

(d)

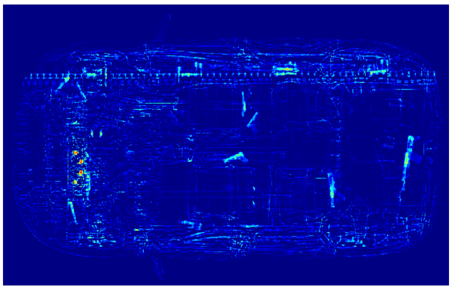

(e)

Fig. 11. (a) ***T*** and ***R*** with a visible strong vertical shift between both images; Difference maps following: (b) rigid registration, (c) 1D horizontal correction, (d) simultaneous registration, (e) horizontal-then-vertical registration with r_α = 1.5, r_β = 2

Table. 4. Mean Square Error measures obtained with the different registration methods

	Rigid Registration	**X-axis Correction**	**X-then-Y Correction**	**Simultaneous**
MSE	3.40E-03	2.80E-03	1.10E-03	2.10E-03

In **Fig. 12.**, an extra visualization enhancement case is described.

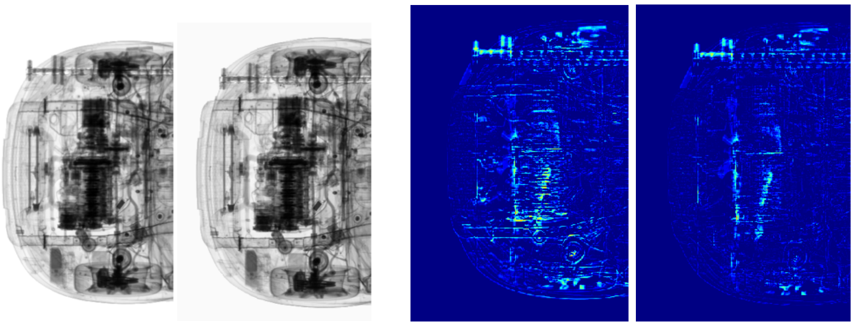

(a) (b) (c)

Fig. 12. (a) $\boldsymbol{R}$ and $\boldsymbol{T}$; Difference maps after: (b) 1D horizontal correction, (c) horizontal-then-vertical elastic registration with r_α = 1.5, r_β = 2. Threat detection capacity is strongly enhanced.

6 Conclusion

In this paper, we address the issue of vertical correction for the registration of x-ray images of same-model vehicles. This correction is particularly necessary whenever a singular vertical translation occurs between the cars in $\boldsymbol{R}$ and $\boldsymbol{T}$. Two approaches are put forward: a simple diffusion paradigm together with a linearized approximation of the smoothly-constrained volume-preserving registration (which turns into the famous elastic registration problem). A discussion is given about applying the registration simultaneously on both components of the displacement field $\boldsymbol{u}$ (with the columnwise-constancy constraint on the horizontal term). The alternative, more efficient method, consists in running the horizontal registration first, followed by the vertical correction in a separate fashion. The results are less noisy, yielding a better registration accuracy on both numerical and visual aspects, especially when elastic regularization is employed.

We also highlight the importance of an appropriate choice for the regularization parameters with the risk of smoothing out suspicious items in the difference map.

Still, resorting to second-order techniques instead of gradient descent methods should be considered for speed purposes. Similarly, matrix-free approaches should also be regarded in future works.

References

1. Modersitzki, J. (2004). Numerical methods for image registration. Oxford University Press on Demand.
2. Modersitzki, J. (2009). FAIR: flexible algorithms for image registration (Vol. 6). SIAM.
3. Marciano, A., Cohen, L. D., & Gadi, N. (2017, June). Vehicle X-ray Scans Registration: A One-Dimensional Optimization Problem. In International Conference on Scale Space and Variational Methods in Computer Vision (pp. 578-589). Springer, Cham.
4. Fischer, B., & Modersitzki, J. (2003). Fast image registration: a variational approach. In Proceedings of the International Conference on Numerical Analysis & Computational Mathematics, G. Psihoyios (ed.), Wiley (pp. 69-74).
5. Haber, E., & Modersitzki, J. (2006). A multilevel method for image registration. SIAM Journal on Scientific Computing, 27(5), 1594-1607.
6. Sotiras, A., Davatzikos, C., & Paragios, N. (2013). Deformable medical image registration: A survey. IEEE transactions on medical imaging, 32(7), 1153-1190.
7. Haber, E., & Modersitzki, J. (2004). Numerical methods for volume preserving image registration. *Inverse problems*, *20*(5), 1621.
8. Haber, E., & Modersitzki, J. (2007). Image registration with guaranteed displacement regularity. *International Journal of Computer Vision*, *71*(3), 361-372.
9. Thirion, J. P. (1998). Image matching as a diffusion process: an analogy with Maxwell's demons. Medical image analysis, 2(3), 243-260.
10. Rohlfing, T., Maurer, C. R., Bluemke, D. A., & Jacobs, M. A. (2003). Volume-preserving nonrigid registration of MR breast images using free-form deformation with an incompressibility constraint. IEEE transactions on medical imaging, 22(6), 730-741.
11. Christensen, G. E., & Johnson, H. J. (2001). Consistent image registration. *IEEE transactions on medical imaging*, *20*(7), 568-582.
12. Rueckert, D., & Aljabar, P. (2015). Non-rigid registration using free-form deformations. In Handbook of Biomedical Imaging (pp. 277-294). Springer US.
13. Younes, L. (2003). Invariance, déformations et reconnaissance de formes (Vol. 44). Springer Science & Business Media.
14. Beg, M. F., Miller, M. I., Trouvé, A., & Younes, L. (2005). Computing large deformation metric mappings via geodesic flows of diffeomorphisms. International journal of computer vision, 61(2), 139-157.
15. Christensen, G. E., Rabbitt, R. D., & Miller, M. I. (1996). Deformable templates using large deformation kinematics. IEEE transactions on image processing, 5(10), 1435-1447.
16. Mang, A., & Biros, G. (2015). An Inexact Newton--Krylov Algorithm for Constrained Diffeomorphic Image Registration. SIAM journal on imaging sciences, 8(2), 1030-1069.
17. Mang, A., & Biros, G. (2016). Constrained H^1-Regularization Schemes for Diffeomorphic Image Registration. SIAM Journal on Imaging Sciences, 9(3), 1154-1194.
18. Hameeteman, R., Veenland, J. F., & Niessen, W. J. (2006). Volume preserving image registration via a post-processing stage. Proceedings of SPIE, 2008 vol. 6288.
19. Fischer, B., & Modersitzki, J. (2008). Ill-posed medicine—an introduction to image registration. Inverse Problems, 24(3), 034008.
20. Rühaak, J., König, L., Tramnitzke, F., Köstler, H., & Modersitzki, J. (2017). A matrix-free approach to efficient affine-linear image registration on CPU and GPU. Journal of Real-Time Image Processing, 13(1), 205-225.
21. Albrecht, T., Dedner, A., Lüthi, M., & Vetter, T. (2013). Finite element surface registration incorporating curvature, volume preservation, and statistical model information. Computational and mathematical methods in medicine, 2013.